

Coherent Adiabatic Spin Control in the Presence of Charge Noise Using Tailored Pulses

Hugo Ribeiro,¹ Guido Burkard,¹ J. R. Petta,^{2,3} H. Lu,⁴ and A. C. Gossard⁴

¹*Department of Physics, University of Konstanz, D-78457 Konstanz, Germany*

²*Department of Physics, Princeton University, Princeton, New Jersey 08544, USA*

³*Princeton Institute for the Science and Technology of Materials (PRISM),
Princeton University, Princeton, New Jersey 08544, USA*

⁴*Materials Department, University of California at Santa Barbara, Santa Barbara, California 93106, USA*

(Dated: July 13, 2012)

We study finite-time Landau-Zener transitions at a singlet-triplet level crossing in a GaAs double quantum dot. Sweeps across the anti-crossing in the low driving speed limit match well with theoretical predictions based on the asymptotic Landau-Zener scattering approach. In particular, we only observe interference fringes when the detuning is swept through the anti-crossing. In contrast, for short rise-time pulses we find oscillations on both sides of the anti-crossing, as expected from finite-time theory. We demonstrate that both of these results are compatible if spin and charge degrees of freedom are taken into account in the time-dependent dynamics. We show that charge noise induces a competing mechanism against Landau-Zener transitions, which can be canceled by choosing appropriately tailored detuning pulses.

The adiabatic theorem of quantum mechanics states that a quantum system will remain in its instantaneous eigenstate if the variation of a dynamical parameter is slow enough compared to the energy separation from other eigenstates [1]. However, there are systems for which adiabaticity breaks down resulting in a transition between states. The first result quantifying population change in such a process is due to independent works by Landau, Zener, Stückelberg, and Majorana [2–5]. They considered a coupled two-level quantum system whose energies are controlled by a time dependent external parameter, which is defined such that the system exhibits an anti-crossing of magnitude $\Delta = 2\lambda$ at $t = 0$. If the system is prepared in its ground state, $|0\rangle$, at $t = -\infty$ and swept through the anti-crossing by modifying the external parameter in such a way that the energy difference is a linear function of time, $\Delta E = \alpha t$, then the probability to remain in $|0\rangle$ at $t = \infty$ is given by $P_{\text{LZSM}} = e^{-\frac{2\pi\lambda^2}{\hbar\alpha}}$, which is known as the Landau-Zener(-Stückelberg-Majorana) (LZSM) non-adiabatic transition probability. Remarkably, this elegant solution, although valid only in the asymptotic limit for an infinitely long sweep, has demonstrated its accuracy in real physical systems for which the sweep has a finite duration [6].

Another success of the asymptotic formulation resides in an accurate description of LZSM interferometry. If the system is driven back and forth across an avoided crossing, it accumulates a Stückelberg phase that gives rise to periodic variations in the transition probability [6]. Although the exact accumulated phase can only be calculated by solving the time-dependent Schrödinger equation [7–10], a scattering approach assimilating the phase acquired in a single passage to a Stokes phase [11] nicely reproduces experimental results obtained in superconducting qubits [12], two-electron spin qubits at a singlet (S)-triplet (T_+) anti-crossing [13, 14], and in nitrogen-

vacancy centers in diamond [15].

Focusing on spin qubits, passage through a S- T_+ anti-crossing in the energy level diagram is analogous to a spin-dependent beam splitter [13]. There are two major challenges relating to quantum control of such systems. First, in two-electron double quantum dots (DQD), the S- T_+ anti-crossing is located near the $(1,1) \leftrightarrow (2,0)$ interdot charge transition, where (N_L, N_R) refer to the number of electrons in the left and right quantum dots. As a result, the singlet state involved in the spin-dependent anti-crossing is a superposition of $(1,1)$ and $(2,0)$ singlet states. Second, the magnitude of the anti-crossing is set by transverse hyperfine fields. To achieve 100% visibility LZSM oscillations, the sweep through the anti-crossing would have to be performed on a timescale set by T_2^* . As a result, there is a tradeoff between adiabaticity and inhomogeneous dephasing. While there are several studies about dissipative adiabatic passages (see for instance [16–19]), it remains to be shown how to make a system less sensitive to dissipation while at the same time increasing adiabaticity.

In this Letter, we attempt to reconcile the contradiction between the need for a slow (adiabatic) passage susceptible to dissipation and a fast passage minimizing dissipation effects. Our approach is based on the observation that the biggest population change occurs in the vicinity of the avoided crossing. We have developed a multi-ramp pulse sequence that has a detuning dependent level velocity, schematically illustrated by the “double hat” pulse in Fig. 1(c). The slow level velocity portion of the pulse is chosen to coincide with the passage through the S- T_+ avoided crossing in order to increase the visibility of the quantum oscillations.

To demonstrate the advantages of tailored pulses, we consider a finite-time LZSM model [20]. In Fig. 1(b), we compare the adiabatic transition probability, P_a , as

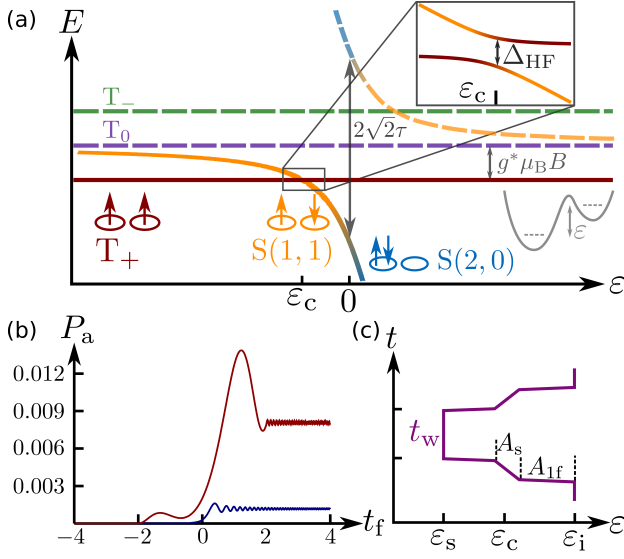


Figure 1. (color online) (a) DQD energy levels as a function of the detuning, ε , near the $(1, 1) \leftrightarrow (2, 0)$ charge transition. The low energy hybridized singlet state and the triplet T_+ form a qubit whose dynamics can be controlled through LZSM interferometry by sweeping the system through the hyperfine mediated avoided crossing. (b) Comparison of the adiabatic transition probability, P_a , for a single pulse with initial propagation time $t_i = -4$ ns, $\alpha = 10^4$ eVs $^{-1}$, and $\lambda = 50 \cdot 10^{-9}$ eV (blue) and a multi-rise time pulse [see panel (c)] with a slow level velocity $\alpha_{\text{slow}} = 10^3$ eVs $^{-1}$ between $t_f = -2$ ns and $t_f = 2$ ns, and $\alpha = 10^4$ eVs $^{-1}$ elsewhere. (c) Sketch of a “double hat” pulse, which consists of fast ramps away from the avoided crossing and a slow ramp in the vicinity of the avoided crossing. The amplitudes of the first fast ramp and the slow ramp are denoted A_{1f} and A_s .

function of final-time, t_f , obtained with single and multi rise-time pulse. To be consistent with the regime experiments are performed in, we choose a weak coupling with $\lambda/\sqrt{\alpha\hbar} \ll 1$. Control of the level velocity in the multi-ramp pulse increases adiabaticity in the vicinity of the avoided crossing. The perfect beam splitter limit corresponds to $P_a = 0.5$. Its achievement would imply the possibility of realizing the Hadamard gate, which is essential to perform certain quantum algorithms (e.g. Shor’s period finding algorithm [21]). Optimization methods to obtain $P_a = 1$ have already been studied [22].

We measure and model LZSM transitions at the S - T_+ anti-crossing for finite duration sweeps. Measurements are performed on a GaAs/AlGaAs heterostructure that supports a two-dimensional electron gas located 110 nm below the surface of the wafer. We use a triple quantum dot depletion gate pattern, where two of the dots are configured in series as a DQD and the third dot serves as a highly sensitive quantum point contact charge detector [13]. The DQD is configured in the two-electron regime, where the electrons can either be separated in the $(1, 1)$ configuration or localized on a single quantum dot,

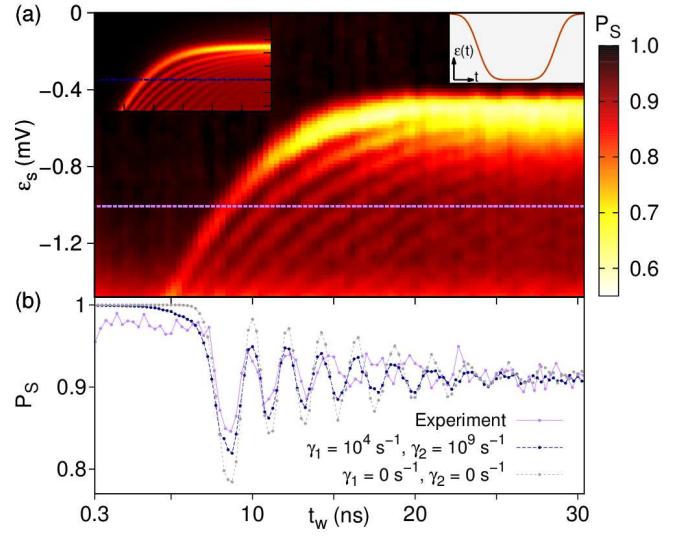


Figure 2. (color online) (a) Singlet return probability P_s plotted as a function of ε_s and t_w for $B = 90$ mT. Upper left inset: theory plot of P_s . Upper right inset: The detuning pulse is obtained by convolving a square pulse with a Gaussian. (b) Comparison of experiment and theory along $\varepsilon_s = -1.008$ mV. Experimental measurements are in purple, theory points obtained via solution of the master equation with $\gamma_1 = 10^4$ s $^{-1}$ and $\gamma_2 = 10^9$ s $^{-1}$ are shown in blue, and theory values obtained with $\gamma_1 = 0$ s $^{-1}$ and $\gamma_2 = 0$ s $^{-1}$ are shown in gray. The good quantitative agreement between experiment and theory including relaxation and charge noise mediated spin dephasing indicates that these phenomena play an important role in the qubit dynamics.

forming the $(2, 0)$ charge state. In this regime, the spin states are the singlets $S(2, 0)$ and $S(1, 1)$ and the $(1, 1)$ triplet states T_+ , T_0 , and T_- . Interdot tunnel coupling τ results in hybridization of the charge states at zero detuning with a resulting splitting of magnitude $2\sqrt{2}\tau$ between a ground and excited state singlet, that we respectively denote S and S' . An external magnetic field is applied perpendicular to the sample, resulting in Zeeman splitting of the triplet states, as depicted in Fig. 1(a). The hyperfine interaction between electron and nuclear spins results in an anti-crossing between S and T_+ located at ε_c . The energy difference at the anti-crossing, Δ_{HF} , is set by transverse hyperfine fields [23].

Simulated interference patterns are obtained by solving the master equation $\dot{\rho} = -\frac{i}{\hbar}[H, \rho] + \frac{1}{2}\sum_{i=1}^3 \left([L_i \rho, L_i^\dagger] + [L_i, \rho L_i^\dagger] \right)$ [24]. Here, the Hamiltonian H describes the dynamics in the vicinity of the $S - T_+$ anti-crossing and is given by [25],

$$H(t) = E_S(t)|S\rangle\langle S| + E_{T_+}(t)|T_+\rangle\langle T_+| + g(t)(|S\rangle\langle T_+| + \text{h.c.}), \quad (1)$$

where E_S is the unperturbed singlet energy, $E_{T_+} = g^* \mu_B (B + B_n^z)$ is the triplet energy, with $g^* = -0.44$ the effective Landé g -factor, μ_B the Bohr magneton, B

the external magnetic field, and B_n^z the z -component of the hyperfine field. The effective coupling $g(t)$ between electronic spin states depends on the hyperfine interaction with nuclear spins and on the charge state. It can be written as $g(t) = c(t)\lambda$, with $c(t)$ the time-dependent (1,1) charge amplitude and λ the hyperfine matrix element between $S(1,1)$ and T_+ . The Lindblad operators L_i are given by $L_1 = \sqrt{\Gamma_+}\sigma_+$, $L_2 = \sqrt{\Gamma_-}\sigma_-$, and $L_3 = \sqrt{\Gamma_\varphi}\sigma_z$. They respectively describe relaxation from excited to ground state and vice versa with rates $\Gamma_- = \gamma_1(n+1)$ and $\Gamma_+ = \gamma_1 n$ due to phonon emission and absorption, with the mean phonon number $n = (e^{\Delta E/k_B T} - 1)^{-1}$ and spontaneous spin relaxation rate $\gamma_1 = 1/T_1$, as well as pure dephasing with a rate Γ_φ . A phenomenological model for the rates leads to the relation $\Gamma_+ + \Gamma_- = \gamma_1 \coth(\Delta E(t)/2k_B T)$, where $\Delta E(t)$ is the energy difference between the instantaneous eigenstates of Eq. (1), k_B is Boltzmann's constant, and T is the electron temperature.

We furthermore assume that pure dephasing is mainly due to charge noise when the qubit is in a superposition of $S(2,0)$ and T_+ . Since these two states have different orbital wave functions, they are sensitive to electric fluctuations of the charge background [26, 27]. We thus assume $\Gamma_\varphi = \gamma_2(1 - |c(t)|^2)$. The rates γ_1 and γ_2 are free parameters and can be used to fit experimental results. Nuclear spin induced dynamics are obtained by averaging solutions of the master equation over a Gaussian distribution of hyperfine fields [26, 28], suitable when the thermal energy is larger than nuclear Zeeman energy, $k_B T \gg g_n \mu_n B$, where g_n is the nuclear g-factor and μ_n is the nuclear magneton. The standard deviation of the distribution of nuclear fields B_n^z along the static external magnetic field is denoted by σ_z . The width of the Gaussian distribution for the hyperfine flip-flop matrix element λ is given by the standard deviation σ_\perp of the nuclear-field distribution perpendicular to the external field. The singlet energy and charge amplitude coefficient used for our simulations are determined experimentally [13].

We first consider spin dynamics in the case of slow rise-time pulses [see inset, Fig. 2(a)]. We model the experimental pulses by convolving a square pulse with a finite rise-time of 1.5 ns, a maximal amplitude of -1.7 mV, and a variable width, with a Gaussian pulse of mean $\mu = 0$ and standard deviation s . We determine $s = 3.7$ ns from the experimentally measured singlet return probability P_S . By monitoring the position of the avoided crossing as a function of waiting time, t_w (width of the pulse), we can extract the relation between the maximal pulse amplitude and waiting time. We assume that for long waiting times, the convolved pulse at the sample still has a maximal amplitude of -1.7 mV. Figure 2(a) shows experimental measurements of the singlet state return probability, P_S , measured as a func-

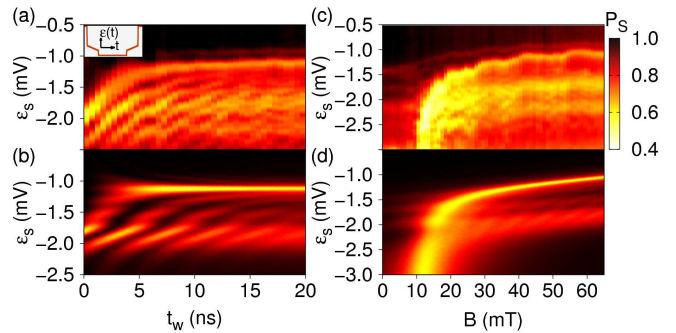


Figure 3. (color online) (a) Measurements of P_S as a function of t_w and ε_s for $A_{1f} = -2$ mV, $t_{\text{slow}} = 4$ ns, and $B = 55$ mT. (b) Theoretical calculations. In comparison with single rise-time pulses, the interference pattern exhibits higher visibility for a range of detunings due to increased adiabaticity resulting from the slow rise-time component of the pulse. Evidence of oscillations can be identified before the anti-crossing, suggesting that only a finite-time LZSM theory is adequate to describe the spin system. (c) P_S plotted as a function of B and ε_s for $t_w = 20$ ns reveals the spin-funnel. Parameters are $A_{1f} = -2$ mV and $t_{\text{slow}} = 4$ ns. Both measurements and theory (d) show indications of finite-time effects.

tion of t_w and ε_s for $B = 90$ mT. The upper left inset in Fig. 2(a) shows theoretical predictions obtained using $\sigma_z = 60$ neV, $\sigma_\perp = 170$ neV, $\gamma_1 = 10^4$ s $^{-1}$, and $\gamma_2 = 10^9$ s $^{-1}$. In Fig. 2(b), we plot P_S as a function of t_w at fixed $\varepsilon_s = -1.008$ mV for experimental data (purple). Theoretical predictions obtained through integration of the master equation are shown in blue and values obtained with no relaxation and no dephasing are plotted in gray.

We find good quantitative agreement between experiment and a theory including spin relaxation (e.g. phonon assisted spin-orbit relaxation) and charge noise induced spin dephasing. These results indicate that the qubit is not only influenced by nuclear spins, but that there are additional physical mechanisms that determine the oscillation visibility. Here, the contrast is also limited due to the superposition of $S(2,0)$ and $S(1,1)$. First, the weighting of $S(1,1)$ sets the amount of population that can be transferred to T_+ . Second, superpositions of different charge states are susceptible to charge noise, which results in an additional effective spin dephasing mechanism. This dephasing channel directly competes against LZSM tunneling by preventing the qubit from coherently interfering with itself. Spin relaxation also changes the balance of populations, but due to energy scales its effect is weak far from the avoided crossing, where $k_B T \ll \Delta E$.

We now consider a detuning pulse which is tailored to have a detuning-dependent level velocity at the leading and trailing edges of the pulse. The voltage pulse profile is shown in the inset of Fig. 3(a). The leading edge of the pulse has a level velocity that varies in the sequence fast-slow-fast. The leading edge has a rise-time of 0.1 ns and

an amplitude A_{1f} , which is followed by a slow ramp with rise-time t_{slow} and amplitude $A_s = -0.5$ mV. A 0.1 ns rise-time pulse shifts the detuning to its maximal value of -3 mV, where the detuning is held constant for a time interval t_w . The trailing edge of the pulse is simply the reverse of the leading edge [c.f. Fig. 1(c)]. In Fig. 3, we compare experiment and theory for $t_{\text{slow}} = 4$ ns, $A_{1f} = -2$ mV.

P_S is plotted as a function of t_w and ε_s for $B = 55$ mT in Fig. 3(a) and (b). A “spin-funnel” that is obtained using the spectroscopy method developed in [29] with a waiting time $t_w = 20$ ns is shown in Fig. 3(c) along with the corresponding theory plot in (d). Parameters used in the theory panels are $\sigma_z = 60$ neV, $\sigma_\perp = 270$ neV, $\gamma_1 = 10^4$ s $^{-1}$ and $\gamma_2 = 10^9$ s $^{-1}$.

Both the experimental results and numerical simulations show enhanced interference visibility within the region between $\varepsilon_s \sim -1.5$ mV and ~ -2.25 mV. From our previous considerations of the finite-time LZSM model, this region should correspond to values of P_S determined by the slow rise-time component of the pulse. The position of the anti-crossing is located at ~ -1.1 mV from the data shown in Fig. 3(a) and (c). Moreover, since $A_{1f} = -2$ mV, $A_s = -0.5$ mV, and the maximal pulse amplitude is -3 mV, the high contrast region should be located between -1.6 mV and -2.1 mV in good agreement with our results.

Our measurements also show evidence of finite-time effects, which have been theoretically predicted [30] but not yet studied in DQD devices. It is possible to identify oscillations in P_S before the avoided crossing in Figs. 3(a) and (b). The range of detunings where finite-time oscillations can be observed is however narrower than previously predicted. This is a consequence of the effective spin coupling which decreases quickly to 0 when the detuning favors $(2, 0)$ states. This also explains variations of P_S before the anti-crossing in spin-funnel measurements, Figs. 3(c) and (d). The observation of finite-time effects implies a dependence of P_S on the propagation times t_i and t_f [20], where $t = 0$ is defined at the anti-crossing. We can verify this behavior by varying A_{1f} , which changes the relative starting and stopping position of the slow rise-time component of the pulse. We consider a second pulse with $A_{1f} = -2.25$ mV, for which the results are presented in Fig. 4.

First, we observe that the high-contrast region is shifted towards more positive detunings, which confirms our previous analysis. Second, we notice the overall difference between the interference pattern in Figs. 3 and 4, panels (a) and (b). This dissimilarity can only be explained by different phase accumulation due to distinct t_i and t_f . In the usual scattering description of LZSM interferometry, the transition probability only depends on the level velocity at the anti-crossing and on the coupling strength. But here, these two quantities have remained unchanged. It is therefore possible to manipulate the

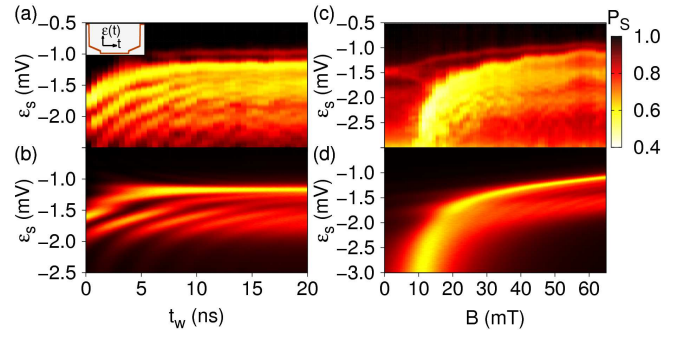


Figure 4. (color online) Experimentally, (a) and (c), and theoretically, (b) and (d), obtained LZS interference patterns and spin-funnels. Here $A_{1f} = -2.25$ mV, $t_{\text{slow}} = 4$ ns, and $B = 55$ mT. The waiting time for the spin-funnel is $t_w = 20$ ns. The interference patterns differ from results presented in Fig. 3, indicating that the evolution of the system is not only sensitive to the level velocity, but also the time at which the change in level velocity happens.

qubit states by keeping a constant driving and instead change the relative starting and stopping position of the detuning pulse.

In conclusion, we have demonstrated how to increase the visibility of quantum oscillations by enhancing the adiabatic passage probability in the presence of dissipation. We have designed a pulse which combines both fast and slow rise-time ramps to respectively minimize dissipation and enhance adiabaticity. By considering a $S-T_+$ anti-crossing, we have shown that it is possible to achieve coherent superposition states with high T_+ population with an unprepared nuclear spin state ($T_2^* \approx 10$ ns). In the more general context of LZSM driven spin qubits, this technique allows one to perform more quantum gates within a given decoherence time and achieve higher amplitude rotations in the qubit space without exponentially extending the gate operation times. Our control technique can be further improved by preparing a nuclear spin gradient [31]. This will not only increase T_2^* , but it will also enhance the effective coupling between spin states, thus boosting adiabatic transition probabilities.

We acknowledge fruitful discussions with David Huse. Research at Princeton is supported by the Sloan and Packard Foundations, the NSF through the Princeton Center for Complex Materials (DMR-0819860) and CAREER award (DMR-0846341), and DARPA QuEST (HR0011-09-1-0007). Work at UCSB was supported by DARPA (N66001-09-1-2020) and the UCSB NSF DMR MRSEC. H. R. and G. B. acknowledge funding from the DFG within SPP 1285 and SFB 767.

[1] M. Born and V. A. Fock, *Zeitschrift für Physik A* **51**, 165 (1928).

- [2] L. D. Landau, Phys. Z. Sowjetunion **2**, 46 (1932).
- [3] C. Zener, Proc. R. Soc. A **137**, 696 (1932).
- [4] E. C. G. Stückelberg, Helv. Phys. Acta **5**, 369 (1932).
- [5] E. Majorana, Nuovo Cimento **9**, 43 (1932).
- [6] S. N. Shevchenko, S. Ashhab, and F. Nori, Physics Reports **492**, 1 (2010).
- [7] H. Ribeiro and G. Burkard, Phys. Rev. Lett. **102**, 216802 (2009).
- [8] J. Särkkä and A. Harju, N. J. Phys. **13**, 043010 (2011).
- [9] G. D. Fuchs, G. Burkard, P. V. Klimov, and D. D. Awschalom, Nat. Phys. **7**, 789 (2011).
- [10] S. A. Studenikin, G. C. Aers, G. Granger, L. Gaudreau, A. Kam, P. Zawadzki, Z. R. Wasilewski, and A. S. Sachrajda, Phys. Rev. Lett. **108**, 226802 (2012).
- [11] R. E. Meyer, SIAM Review **31**, 435 (1989).
- [12] W. D. Oliver, Y. Yu, J. C. Lee, K. K. Berggren, L. S. Levitov, and T. P. Orlando, Science **310**, 1653 (2005).
- [13] J. R. Petta, H. Lu, and A. C. Gossard, Science **327**, 669 (2010).
- [14] L. Gaudreau, G. Granger, A. Kam, G. C. Aers, S. A. Studenikin, P. Zawadzki, M. Pioro-Ladrière, Z. R. Wasilewski and A. S. Sachrajda, Nat. Phys. **8**, 54 (2012).
- [15] P. Huang, J. Zhou, F. Fang, X. Kong, X. Xu, C. Ju, and J. Du, Phys. Rev. X **1**, 011003 (2011).
- [16] P. Ao and J. Rammer, Phys. Rev. Lett. **62**, 3004 (1989).
- [17] E. Shimshoni and Y. Gefen, Ann. Phys. **210**, 16 (1991).
- [18] P. Nalbach and M. Thorwart, Phys. Rev. Lett. **103**, 220401 (2009).
- [19] P. P. Orth, A. Imambekov, K. Le Hur, Phys. Rev. A **82**, 032118 (2010).
- [20] N. V. Vitanov and B. M. Garraway, Phys. Rev. A **53**, 4288 (1996).
- [21] P. Shor, SIAM Journal of Computing **26**, 1484 (1997).
- [22] B. T. Torosov, S. Guérin, and N. V. Vitanov, Phys. Rev. Lett. **106**, 233001 (2011).
- [23] J. M. Taylor, J. R. Petta, A. C. Johnson, A. Yacoby, C. M. Marcus, M. D. Lukin, Phys. Rev. B **76**, 035315 (2007).
- [24] G. Lindblad, Commun. Math. Phys. **48**, 119 (1976).
- [25] H. Ribeiro, J. R. Petta, and G. Burkard, *manuscript in preparation*.
- [26] W. A. Coish and D. Loss, Phys. Rev. B **72**, 125337 (2005).
- [27] X. Hu and S. Das Sarma, Phys. Rev. Lett. **96**, 100501 (2006).
- [28] A. V. Khaetskii, D. Loss, and L. Glazman, Phys. Rev. Lett. **88**, 186802 (2002).
- [29] J. R. Petta, A. C. Johnson, J. M. Taylor, E. A. Laird, A. Yacoby, M. D. Lukin, C. M. Marcus, M. P. Hanson and A. C. Gossard, Science **309**, 2180 (2005).
- [30] H. Ribeiro, J. R. Petta, and G. Burkard, Phys. Rev. B **82**, 115445 (2010).
- [31] S. Foletti, H. Bluhm, D. Mahalu, V. Umansky, A. Yacoby, Nat. Phys. **5**, 903 (2009).